Available online at www.sciencedirect.com
ScienceDirect
Trans. Nonferrous Met. Soc. China 30(2020) 1743−1755
Transactions of Nonferrous Metals Society of China
www.tnmsc.cn

Characterization of aluminum based functionally graded composites developed via friction stir processing

Venkatesh BIKKINA, Sadasiva Rao TALASILA, Kumar ADEPU

Department of Mechanical Engineering, National Institute of Technology, Warangal 506004, Telangana, India

Received 2 October 2019; accepted 2 June 2020

Abstract: Al/SiC functionally graded material (FGM) was developed through a novel multi-step friction stir processing (FSP) method. SiC particles with a mean size of 27.5 μm were embedded in the groove on the 6082-Al plate. To create a graded structure over a predefined value, FSP was carried out with three tools with different pin lengths and with varying volume fractions of SiC particles. The structure was formed by passing tools with 1−3 passes with a constant rotational and traveling speeds of 900 r/min and 20 mm/min, respectively. The experiments were conducted at room temperature. Microstructural features of functionally graded (FG) samples were examined by using scanning electron microscopy (SEM) and 3D light microscopy. Mechanical properties in terms of wear resistance and microhardness were thoroughly assessed. The results indicate that the increase in FSP pass number causes more uniform SiC particle dispersion. The microhardness values were impacted by the number of passes and improved by 51.54% for Pass 3 when compared to as-received 6082-Al. Wear resistance of Al/SiC FG samples was found to increase as a result of the addition of SiC particles.

Key words: functionally graded composites; friction stir processing; silicon carbide; AA6082-T6; number of passes

1 Introduction

Functionally graded materials (FGMs) comprise a new class of engineering materials that exhibit spatial gradation in composition and/or structure with respect to preferred orientation. The gradual variation enables the production of superior mechanical properties without any poor interface. It eliminates sharp interfaces (which lead to failure) that exist in traditional composite materials [1]. As a result, such materials have the potential to minimize thermal and residual stress concentrations in various engineering processes and service environments [2]. With the help of FGM, designers can tailor the material responses accordingly to satisfy design criteria. The unique characteristic feature of FGM is its ability to customize material for specific functions and applications. FGM finds wide applications in defense, medical, aerospace, optoelectronics sectors/industries etc. [3−5].

There are various processing methods to produce FGM, namely powder metallurgy (PM) technique [6], centrifugal casting process [7], physical/chemical vapor deposition processes (PVD/CVD) [8], solid free-form fabrication (SFF) process [9], 3D printing [10], and friction stir processing (FSP) [11], etc. Powder metallurgy is one of the most viable methods for processing FGM. It is easy to control the composition, microstructure and form FGM though there are some drawbacks in this route of production, such as adverse microstructural characteristics, porosity, and interfacial reaction. It is possible to create a graded structure by this method but the continuous gradient of composition cannot be achieved [12]. PVD and CVD methods are used for producing thin FGM. They are energy-consuming and release toxic

Corresponding author: Venkatesh BIKKINA; E-mail: venkateshb@student.nitw.ac.in
DOI: 10.1016/S1003-6326(20)65335-3

gases as by-products [13]. The centrifugal casting process is one of the simplest and most cost-efficient methods. However, this method is regulated by segregation which is time-consuming with low quality of gradation control. Another concern with this method is that only axisymmetric parts can be manufactured [14]. Solid free-form fabrication (SFF) is a new class of direct manufacturing process that produces three-dimensional parts from a computer model but the problem is a poor surface finish, which requires secondary finishing operation [15].

Recently, FSP has been proven to be effective and versatile for producing surface composites and localized functional gradient on a micro-scale [16,17]. This is carried out under the same conditions as friction stir welding (FSW). The theory and concept behind the two processes (FSP and FSW) are the same, but the goals are different. FSW is a joining process; whereas FSP is a surface modification process employed for microstructural refinement of workpiece material [18]. FSP has also been widely used to create surface metal matrix composites (MMC) where severe plastic deformation is caused by enforcing a non-consumable stirring tool on the workpiece surface. The FSP method is mainly controlled by the rotational and traveling speeds of the tool. FSP can also be used to fabricate FGM wherein the reinforcement particles are packed in a groove in which the stirring process is performed [19].

There exist a few approaches to the fabrication of composites using FSP. HANGAI and OBA [20] utilized FSP for manufacturing functionally graded aluminum (FG/Al) foams with varying pore structures and concluded that Mg composition has gradually changed in the bonding region. GANDRA et al [21] developed aluminum-based functionally graded MMC by incorporating ceramic particles with different median sizes in the surface layer of aluminum and showed that sufficient particle dispersion takes place when the particles are compacted in a groove located under the probe.

MISHRA et al [22] used a novel method of surface modification process to create a surface composite (Al/SiC) through FSP. They reported that particles reinforced with 27 vol.% of SiC particles exhibit a hardness around HV 173 which is almost double the hardness of parent alloy (5083-Al). MIRANDA et al [23] adopted the FSP technique by employing a consumable tool with prefilled ceramic particles to produce Al-based FGM. The investigation has proved that FSP with a consumable tool approach leads to the formation of a thin composite layer with low time consumption and tool wear.

MORADI FARADONBEH et al [24] performed a study on friction stir welding (FSW) of Al−B_4C composite with 4 different pin geometries and established that FSW parameters have a significant effect on the fragmentation and distribution of reinforcing particles in the weld center. PAIDAR et al [25] conducted FSW to AA5182 by employing tungsten carbide (WC) as a reinforcement particle and concluded that mechanical properties (hardness and tensile) and wear resistance increased due to the addition of WC particles, causing substantial grain growth in the nugget zone.

POL et al [26] developed an effective technique for improving ballistic resistance by incorporating particles of TiB_2 and B_4C in different mass fractions into the surface of AA7005 using FSP. They concluded that the enhancement of ballistic resistance is ascribed to the availability of hard reinforcing particles in the surface composite and matrix tough core. SHARMA et al [27] fabricated Al−B_4C mono and Al−(B_4C+MoS_2) surface hybrid composites in AA6061 with the help of multi-pass FSP and reported that mono surface composite enhanced the hardness where the hybrid surface composite exhibited enhanced wear resistance.

PAIDAR et al [28] produced composite via FSP with a 10-cycle accumulative roll bonding. The researchers observed that by increasing the number of passes (1−8) the homogeneity of B_4C in the Al matrix improved the microstructure, mechanical properties, wear and fracture behavior. GANGIL et al [29] investigated the FSW of hybrid composites produced by FSP on Al−Zn−Mg−Cu alloy (AA7050-T7451). The findings indicated that when compared to composites prepared by FSP, composites welded by FSW showed an increase in microhardness because of better and homogeneous reinforcement particle distribution.

JAIN et al [30] investigated the effect of multi-pass FSP on the mechanical and microstructural properties of AA1050/TiO_2 surface composite. The results revealed that surface composites processed

by the second pass exhibit better wear resistance and hardness caused by acceptable distribution of particles when compared with as-received aluminum. SINGH et al [31] applied FSP to produce FGM with a combination of different matrix materials which are 6063-Al and 8011-Al alloys reinforced with Al_2O_3 and rice husk ash (RHA). The results revealed that tensile strength of hybrid functionally graded material composite increased till it touched 29.54% vis-a-vis 6063-Al alloy as base material and 42.5% in the case of 8011-Al alloy. The surface hardness of the FGM composite is enhanced by 72.5% and 97.11% with regard to base material 6063-Al and 8011-Al alloys, respectively.

BARATI et al [32] used two surface processing methods, i.e., FSP and modified friction stir vibration-assisted processing (FSVP) to fabricate surface composite of Al6061/SiO_2. The mechanical, corrosive and wear properties of surface composite prepared by FSVP were superior to those prepared by FSP due to the formation of small grains and more homogenous distribution of the strengthening particles as the vibration was applied.

The present work sought to address the problem of incorporating reinforcement particles in the base matrix to create a microstructural gradient along the depth. The authors of this work attempted to develop a novel method of tailor-made functionally graded Al/SiC composite by placing SiC particles in pre-prepared square-shaped grooves and systematically evaluated its microstructural characteristics, mechanical properties (mainly wear behavior and microhardness) and correlated them with pass number.

2 Experimental

6082-T6 aluminum alloy rolled plates with the dimensions of 215 mm × 145 mm × 6 mm chemically represented in Table 1 were used as base material (matrix). Silicon carbide (SiC) powder with a mean size of 27.5 μm was selected as reinforcement particles with microstructure as shown in Fig. 1. The tools used for the experiment are made of H13 tool steel. The geometric features of tools are shown in Fig. 2, with different pin lengths of 5.2, 3.2 and 1.7 mm for Tool A, Tool B and Tool C respectively. All the tools have the shoulder diameter equal to 24 mm. Each pin with conical in shape, has a threaded profile, with top and bottom ended diameters 6 and 8 mm, respectively.

Table 1 Chemical composition of 6082-T6 aluminum alloy (wt.%)

Mg	Mn	Fe	Si	Cu	Cr	Al
0.82	0.61	0.29	0.82	0.1	0.23	Bal.

The FSP was performed on the FSW machine (NCFSW−3T) with an automated numerical control system for both rotational and traveling speeds of the tool. The rotational and traveling speeds were set to be 900 r/min and 20 mm/min, respectively. The inclination of the axis of the tool to the vertical axis on the surface plate was set to be 1°. To analyze the influence of multi-pass friction stir processing, the samples were subjected to 1−3 passes.

The schematic representation of fabrication process of a functionally graded (FG) samples by FSP is schematically illustrated in Fig. 3 and

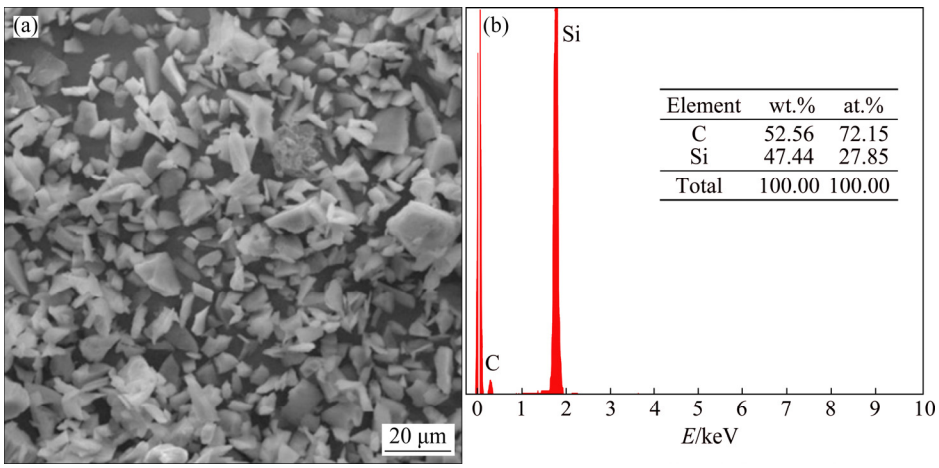

Fig. 1 SEM image (a) and EDS spectrum (b) of as-received SiC particles

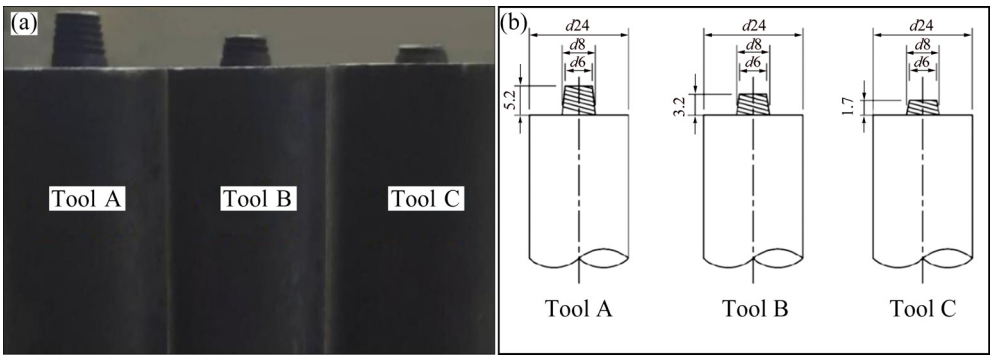

Fig. 2 Geometries (a) and dimensions (b) of FSP tools (unit: mm)

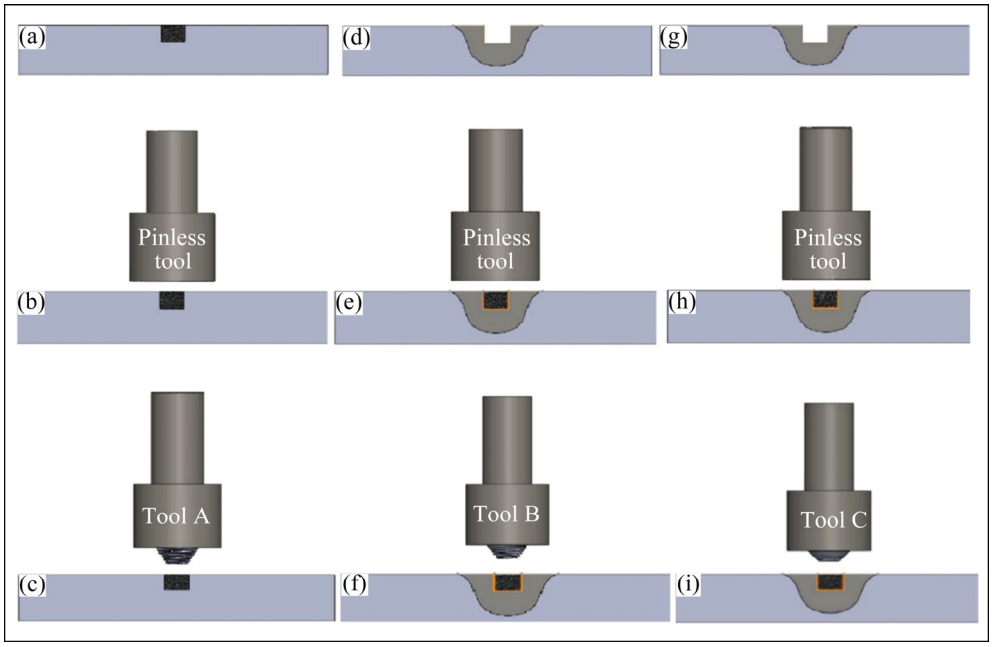

Fig. 3 Schematic representation of fabrication process of FG composite via FSP: (a) Groove filled with SiC particles; (b) Sealing of groove using pinless tool; (c) Processing of composite (Region 1) using Tool A; (d) Secondary groove filled with SiC particles; (e) Sealing of secondary groove using pinless tool; (f) Processing of composite (Region 2) using Tool B; (g) Filling of SiC particles in tertiary groove; (h) Tertiary groove sealed using pinless tool; (i) Processing of composite (Region 3) using Tool C

comprises the following steps. At first, the groove was made on the 6082-Al plate with a width and a depth of 1.5 and 5 mm, respectively, using wire cut electric discharge machining (EDM) compacted with 6 vol.% of SiC particles. After filling with SiC particles, a pin-less tool was used to seal the top surface of the groove, and to prevent the sputtering of reinforcement particles during processing. Once the groove was sealed, the samples (6082-Al plate) were subjected to different pass numbers of 1−3 with Tool A. To form the FG composite, the processed zone was again grooved with the width and depth of 0.5 and 3 mm, respectively. Subsequently, it was filled with 8 vol.% (cumulative) of SiC particles and sealed. Following this, the sample was again processed with Tool B and grooved once again with the width and depth of 0.6 and 1.5 mm, respectively. It was packed with 10 vol.% (cumulative) of SiC particles and sealed. As a final step in the processing, the sample was processed with Tool C.

The fabricated FG samples were sectioned normally to the processing direction and polished mechanically with different grades of SiC abrasive papers. The etching was done with Keller's reagent at room temperature till the preferred contrast was

attained. The microstructural features of FG samples were examined by a 3D light microscopy and scanning electron microscopy (SEM) equipped with an energy-dispersive X-ray spectroscopy (EDX). The Vickers hardness of the FG sample was evaluated across the cross-section of the stir zone (SZ) with a load of 0.98 N for 10 s.

Wear tests were carried out with a pin-on-disc test machine following ASTM G99—04 standard by volume loss approach. The sample to be tested was cut from the SZ with a diameter of 10 mm. The counterpart material was made of EN31 hardened steel with a hardness of HRC 62. In each test, an emery paper with 80 grit size (50 mm in diameter) was mounted on the sliding track to act as an abrasive medium. The wear test was performed without lubrication at a constant load of 15 N and a sliding distance of 75 m. All the test samples and discs were cleaned thoroughly in acetone before and after the wear test.

The wear rate was determined by

$$W_{\mathrm{v}}=\frac{\Delta V}{S} \tag{1}$$

where W_{v} is the volumetric wear rate in mm^3/m, ΔV is the volume loss in mm^3, and S is the sliding distance in m.

Finally, the surface morphology of worn-out FG samples was characterized microscopically by using SEM.

3 Results and discussion

3.1 SiC particle distribution

Figure 4 illustrates a cross-sectional macrograph of the FG composite in which there is a gradation of the volume fraction of the SiC along the thickness direction. Moreover, it is revealed that good bonding between layers is attained, and no cracks are observed in the microstructure. A typical network structure is observed where SiC particles are dispersed throughout the matrix phase. The dispersion of SiC particles is found to be in a gradient manner. The FG sample consists of three regions from top to bottom, namely: (1) Region 1, the SiC rich region (10 vol.%), in which 6082-Al serves the purpose of a matrix phase; (2) Region 2, the continuous transition of the FG sample can be found in the SiC moderate region with a decreasing trend from 8 to 6 vol.%; (3) Region 3, lower region with an average composition of 6 vol.% of SiC. The formation of graded regions from Regions 1 to 3 is due to the multiple passes of Tools A, B and C, respectively.

Microstructures of FG samples (A, B and C) fabricated with 1−3 passes were observed through SEM in different regions. These are depicted in Fig. 5. It is confirmed that a significant amount of SiC particles exist over matrix in FG composite and some fine and coarse SiC particles can be observed in the processed region. The EDAX analysis results of Sample C (Fig. 5(c)) are shown in Fig. 6. It can be seen that elements C, O, Al, Si and Fe were detected in all selected regions of Sample C. In the selected region EDAX, it is found that oxygen content is over 4 wt.% which is due to the decomposition of organic substance (acetone) under electron beam irradiation. When aluminum is exposed to the atmosphere it oxidizes quickly by forming an Al_2O_3 layer on the surface of the aluminum. In addition to the existing phenomenon, it is also observed that the content of SiC gradually decreases from Regions 1−3.

To understand the distribution of SiC particles it is necessary to find the content change in different regions. For this, phase fraction analysis was done using SEM images in different regions of an individual FG sample. Leica app suite 4.8 was used [33] to process the SEM images which are shown in Fig. 7. When the phase fractions for all three passes are compared, it is observed that Pass 3 has a better distribution of SiC particles than Passes 1 and 2. From Table 2 and Fig. 5(c) it is clear that Pass 3 disintegrates the SiC particles finely and this

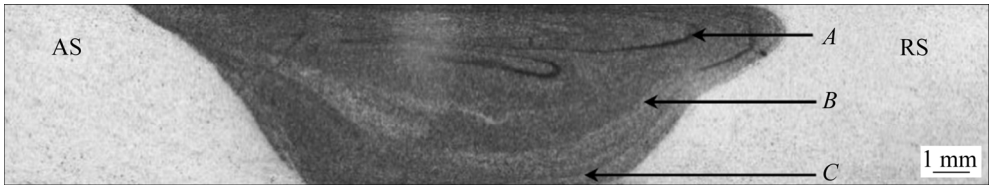

Fig. 4 Macrograph of cross-sectioned Al/SiC FG composite: *A*—SiC rich region (Region 1); *B*—SiC moderate region (Region 2); *C*—SiC lower region (Region 3); AS—Advancing side; RS—Retreating side

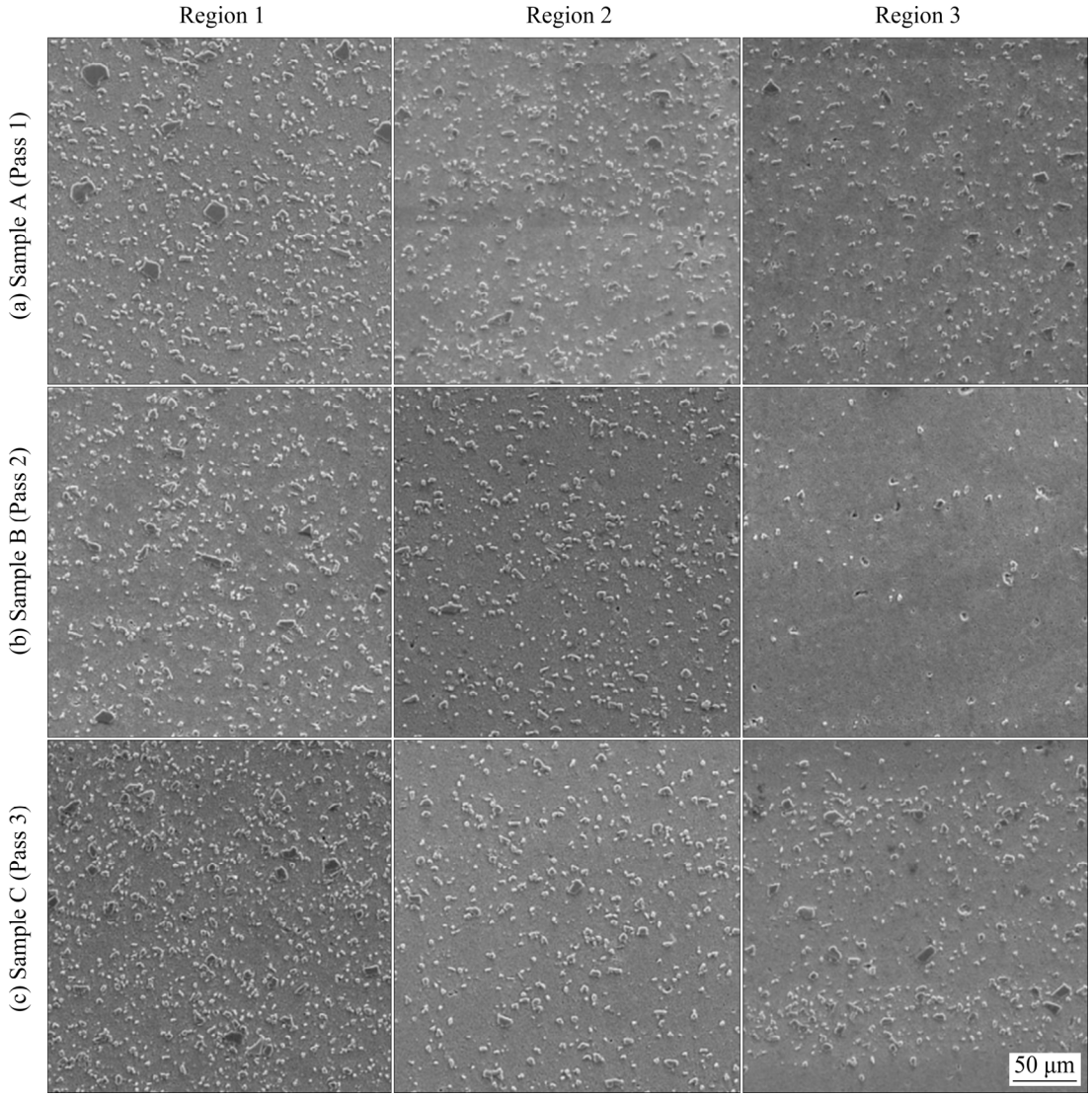

Fig. 5 SEM images showing microstructure of Al/SiC FG composite in different regions fabricated by one FSP pass for Sample A (a), two FSP passes for Sample B (b), and three FSP passes for Sample C (c)

results in SiC phase distribution in Regions 1, 2 and 3, being (17.03±0.8), (12.19±0.2) and (6.75±0.7) vol.%, respectively. Similarly, as FSP passes increase the size of SiC particles decreases, which is discussed in the next section.

3.2 Microstructure

Figure 8 represents the microstructures of the FG samples in which SiC particles were embedded into the surface of the aluminum alloy. In FSP, the formation of fine and equiaxed grains within the SZ is due to the occurrence of dynamic recrystallization (DRX) caused by the local pinning effect [34,35]. The intense plastic deformation within the SZ causes the fragmentation of grains which is usually referred to as dynamic recrystallization. Based on material transport and tool action, the processed area is divided into 3 distinct zones: (1) SZ, (2) thermo-mechanically affected zone (TMAZ) and (3) heat-affected zone (HAZ) [36].

The SZ shown in Fig. 8(a) is for Sample A of Pass 1. It can be seen that the shape of SZ is asymmetric from the center because the SiC particles have transported to the AS compared to the RS. The plastic deformation zone is inadequate for the formation of SiC particle recirculation flow because there is short interaction time between workpiece and tool [37]. The grains formed are with a large area of grain boundaries. The surface composite layer is formed by the first-pass showing particle agglomeration on the surface.

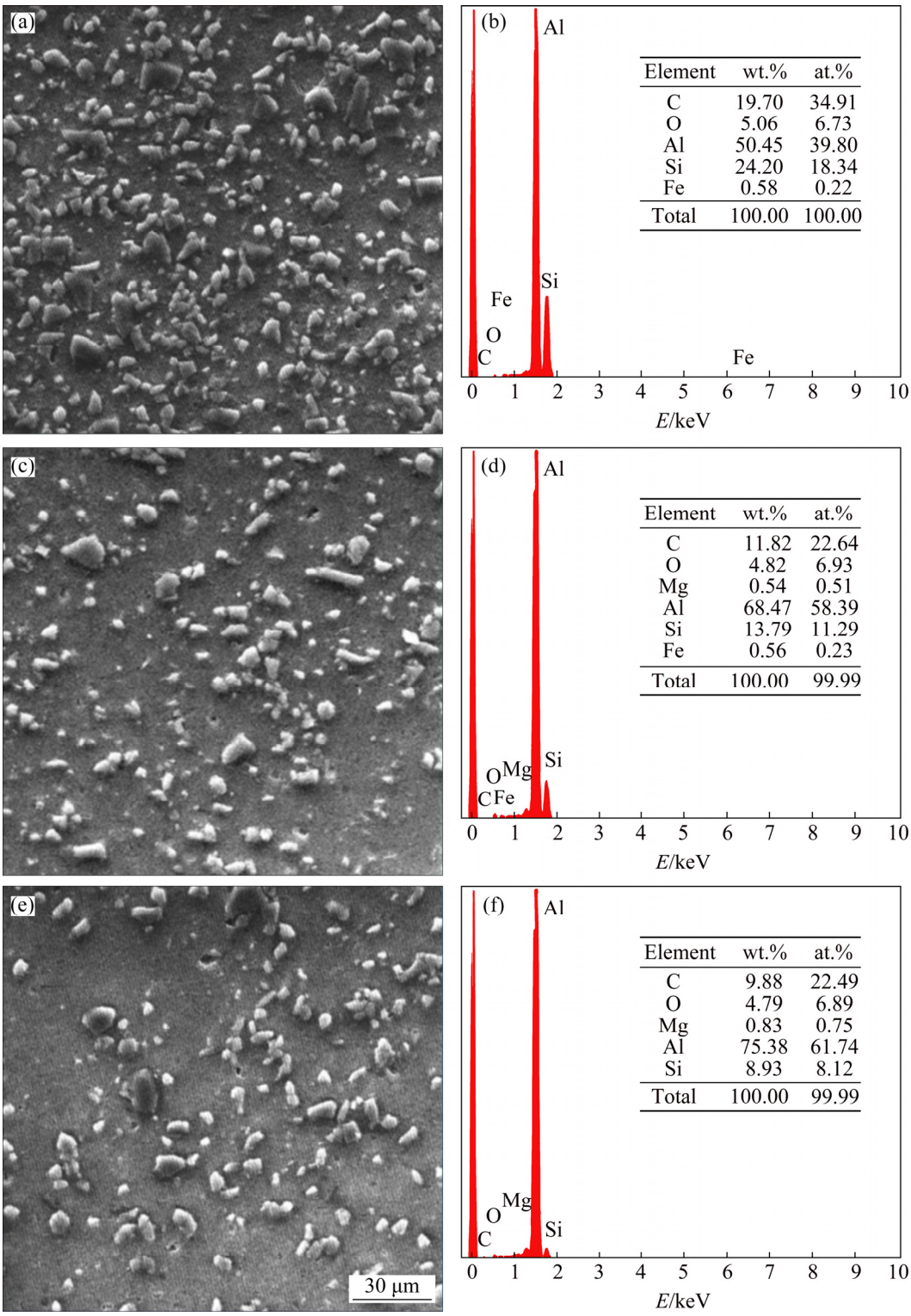

Fig. 6 EDAX analysis of Sample C taken from Region 1 (a, b), Region 2 (c, d) and Region 3 (e, f) in Fig. 5

However, when the number of FSP passes is increased, particle dispersion is found to be more homogenous and any clusters of SiC particles that remain are broken, leading to the creation of a higher number of SiC–Al alloy matrix interfaces. During the second pass, the particle dispersion becomes more uniform (Fig. 8(b)) when compared to the first pass and the cluster size of SiC is reduced while dispersion in upper and lower regions of the SZ is not homogenous, which indicates that stirring action is insufficient to get the uniform particle dispersion.

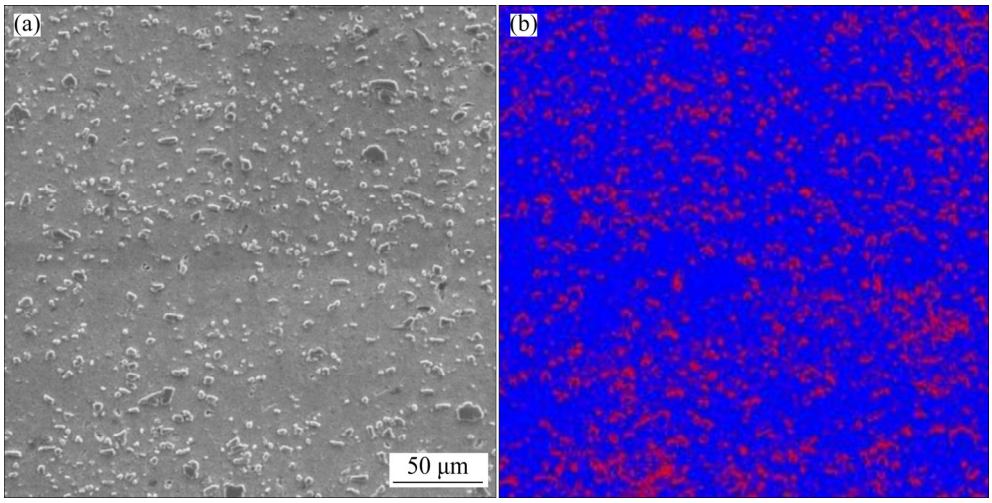

Fig. 7 Images during phase fraction analysis for Sample B in Fig. 5(b): (a) Raw image of Pass 2 in Region 1; (b) Processed image of Pass 2 in Region 1

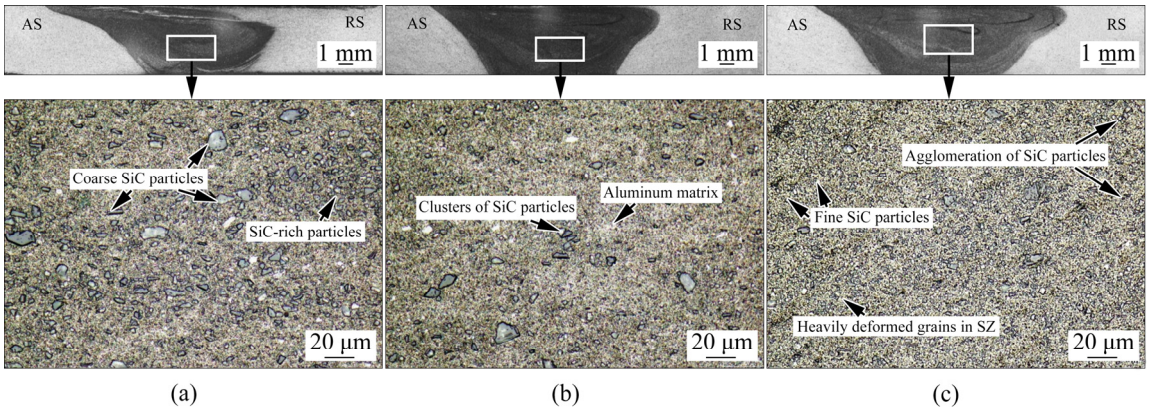

Fig. 8 Microstructures of Al/SiC FG composite near SZ produced by one FSP pass for Sample A (a), two FSP passes for Sample B (b), and three FSP passes for Sample C (c)

Table 2 Comparison of phase fraction in different regions of Sample C in Fig. 5(c) with different FSP passes

Pass No.	Al alloy content/vol.%			SiC content/vol.%		
	Region 1	Region 2	Region 3	Region 1	Region 2	Region 3
1	85.97±0.3	88.50±0.1	90.82±0.4	14.03±0.3	11.50±0.1	9.18±0.4
2	87.62±0.6	89.37±0.5	97.15±0.3	12.37±0.6	10.63±0.5	2.85±0.3
3	82.97±0.8	87.81±0.2	93.25±0.7	17.03±0.8	12.19±0.2	6.75±0.7

To further improve the distribution of particles in the upper and lower regions of the SZ, the third pass is required. Figure 8(c) shows the microstructure of the SZ produced with the third pass where micro-clusters of SiC cannot be seen anymore in the sample with refined structure and without defects. The dispersion of particles is more uniform in the upper and lower regions of the SZ. In addition, symmetric basin shape of the SZ was observed on both the AS and RS, representing homogenous as well as uniform deformation within the SZ. These results show that the morphology of the tool and pass number play an important role in the grain size of SZ.

3.3 Effect of pass number on particle size

Figure 9 presents the effect of pass number on the average size of grain in FG samples produced by FSP. The average size of grain in base metal is approximately 34 μm in as-received condition. In

the FG samples, a fine equiaxed grained structure is obtained with a size ranging from 5.3 to 10.1 μm.

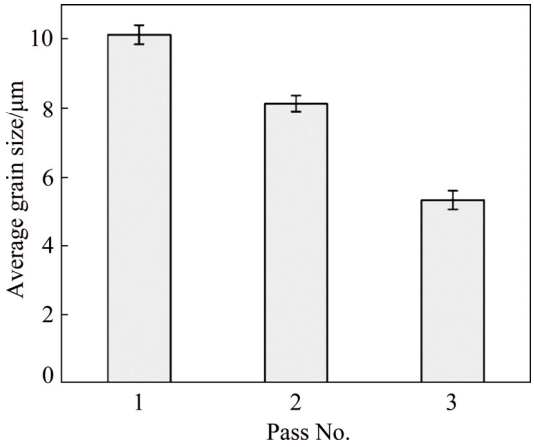

Fig. 9 Average grain size of FG composite as function of FSP pass number

The primary reason for grain refinement is the occurrence of recrystallization and, subsequently, the grain growth hindered by the pinning action of the intermetallic particle. The particles serve as suitable sites to nucleate new grain through particulate stimulated nucleation (PSN) during discontinuous dynamic recrystallization and then, the movement of the grain boundary is reduced by the Zener pinning mechanism [38,39]. Therefore, two mechanisms contribute to achieving significant grain refinement during FSP.

It is noteworthy that, the increase in FSP passes results in refinement and homogenous dispersion of reinforcement particles in the SZ [40]. However, FSP also has a major impact on grain growth due to the accumulation of heat in each FSP pass. It is hypothesized that threaded pins are also responsible for temperature and effective flow of material around the tool [41].

In the first pass the grains were fragmented to form fine grains with an average size of 10.1 μm and were severely broken by FSP into 8.13 μm (in the second pass). Thereby, in the post two passes the grain size was refined to a size about 76.1% smaller than that of the actual grain. It is evident that in the first and second passes, insufficient heat input and improper recrystallization cause the formation of coarser grains. However, it is clear that, in the third pass due to sufficient plastic deformation in the SZ finer grains (5.3 μm) can be obtained.

3.4 Microhardness

Figure 10 depicts Vickers hardness data with varied positions for FG samples along the thickness direction from Region 1 to Region 3. The average microhardness value of 6082-Al (as-received material) was around HV 97. The hardness was observed to decrease gradually along the direction of the gradient from the SiC rich region (Region 1) to the SiC lower region (Region 3).

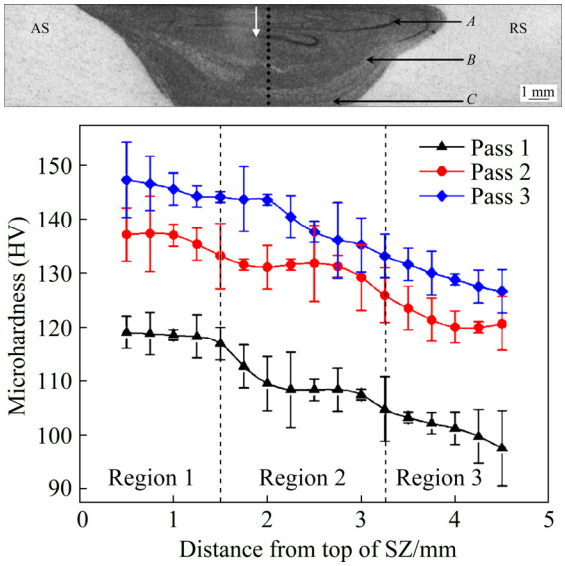

Fig. 10 Microhardness profiles of Al/SiC FG composite in transverse section of SZ for various passes: *A*—SiC rich region (Region 1); *B*—SiC moderate region (Region 2); *C*—SiC lower region (Region 3)

It was interesting to observe that, hardness values of FG samples increased proportionally with the increasing addition of SiC particles. The FG composite surface layer (Fig. 10) in Region 1 along the longitudinal direction containing 10 vol.% SiC displayed the highest value of microhardness of approximately HV 147. This was found to be 1.5 times as higher as that of the as-received material (HV 97). In Region 2 the microhardness of the FG composite surface layer containing 8 vol.% SiC was HV 137, which was lower than that of Region 1. The hardness value of 6 vol.% SiC in Region 3 has drastically reduced to HV 119 due to high inter-particle spacing, non-uniform dispersion of SiC particles and stirring of large grains.

The number of passes played a significant role in the microhardness results. It was found that the microhardness values were affected by the number of passes and improved by 22.68% for Pass 1, 41.24% for Pass 2, and 51.54% for Pass 3,

respectively when compared to as-received material. In the first pass, the hardness value measured in the SZ had increased from HV 97 to HV 119 because of induced development of strain and pinning effect of SiC particles. A further increase in the microhardness for the second pass (HV 137) was observed in the SZ of FG sample because of a reduction in the size of the particles, leading to the even distribution of particles and thus enhancing the hardness values. The third pass showed a higher hardness value of HV 147 because of the fine and uniform dispersion of SiC particles in the matrix. The microhardness results corroborated the microstructural observation in the SZ.

The improvement in the hardness can be attributed to grain size refinement which was caused by dynamic recrystallization along with the Orowan strengthening effect [42]. Due to the difference in thermal expansion coefficients between 6082-Al (matrix) and SiC (reinforcement), the dislocation density was improved, causing an increase in the hardness. Therefore, hardness improvement on the Al/SiC FG samples was caused by the number of passes, microstructural refinement and dispersion of SiC particles.

3.5 Wear behavior

The wear tracks of FG samples observed on the surface after dry sliding tests were analyzed using SEM as shown in Fig. 11. Figure 12 shows the graphical plots of the average wear rate with respect to the number of passes. The SiC particles are usually present over the surface and protect the matrix from functional contact with the counter body surface. Therefore, the interaction between the surfaces is mainly between the protruding SiC particles and the counter body surface, leading to a low wear rate. As mentioned in the earlier section, the variables which enhance the properties of FG composite decrease the wear rate. According to Archard's wear equation, the material hardness is inversely correlated to the wear rate, i.e., wear rate decreases with an increase in hardness [43].

Figure 11(a) presents the morphology of the worn surface of FG samples with Pass 1. In the initial wear stage, a small amount of material was eroded from the FG Sample A and accumulated on the counter surface. The wear mode here seems to be adhesive. On observing the worn surface it was found to be non-uniform with grooves blended at the edges. The reason for the formation of blended grooves was the presence of reinforcing particles. This, therefore, indicates the phenomenon of abrasion. From the above results, it is clear that the

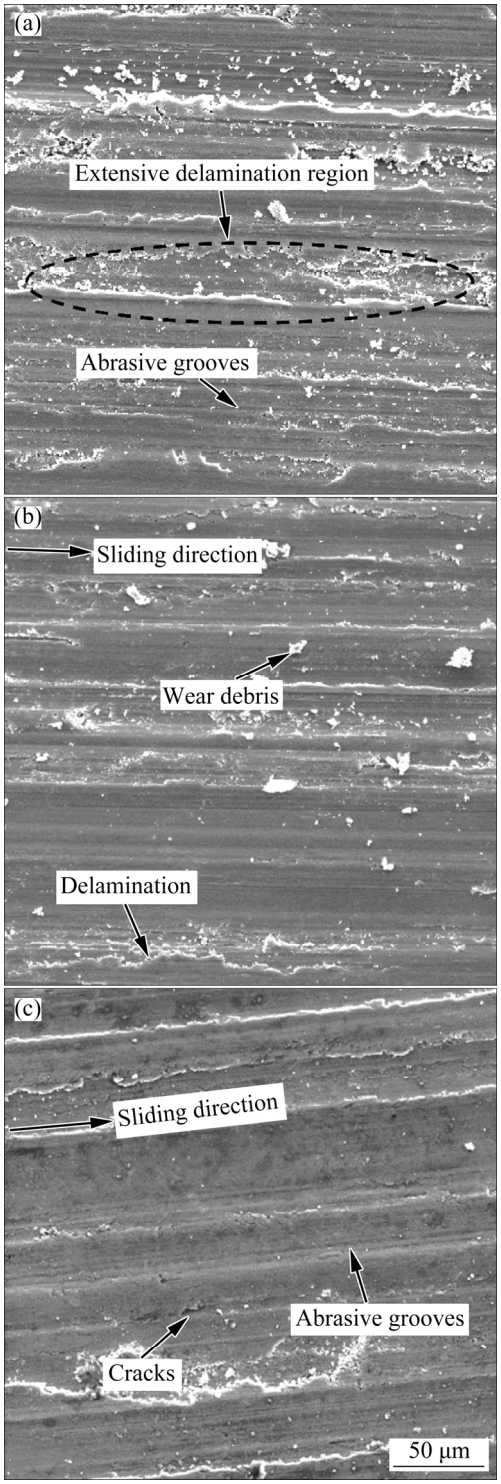

Fig. 11 SEM images of worn surface of Al/SiC FG composite layer fabricated by different FSP passes: (a) Pass 1; (b) Pass 2; (c) Pass 3

wear mechanism on FG composite is an amalgamation of abrasive and adhesive wear modes.

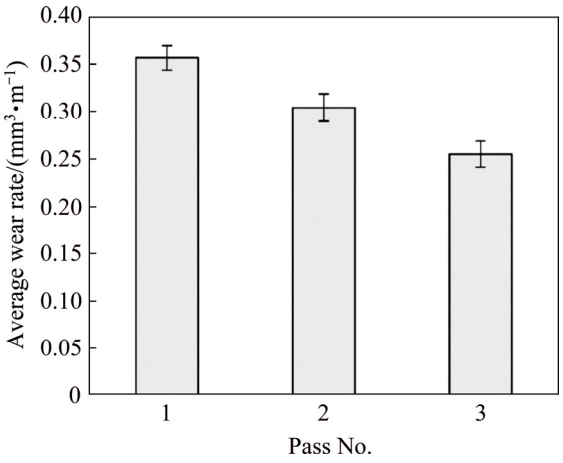

Fig. 12 Correlation between average wear rate and FSP pass number for Al/SiC FG composite

As shown in Fig. 11(b), the width of wear track in the FG Sample B (Pass 2) decreases compared to that of FG sample A (Pass 1). It is evident that the wear rate in Sample B is lower than that in Sample A. The wear track reveals that there are minor pits on the surface, mainly because of the local extraction of ceramic particles. The worn surface exhibits irregular delamination wear, leading to a subsurface crack that grows progressively and eventually shears onto a surface, forming a thin layer.

FG Sample C (Pass 3) with fine grooves and small delamination (Fig. 11(c)) has the lowest wear rate compared to FG Samples A and B. Table 3 shows the average wear rates of FG samples at different pass numbers. A thorough evaluation of the microstructure of the worn surfaces can suggest that wear resistance of FG Sample C is improved due to the increase in the hardness, homogenized distribution of SiC particles in the matrix and strong integration between matrix (aluminum alloy) and reinforcement particles (SiC).

Table 3 Average wear rates of FG samples at different passes

Sample No.	Pass No.	Wear rate/(mm^3·m^{-1})			
		Trial 1	Trial 2	Trial 3	Average
A	1	0.3543	0.3345	0.3482	0.3456
B	2	0.3011	0.3201	0.2915	0.3042
C	3	0.2676	0.2532	0.2454	0.2554

4 Conclusions

(1) Varying SiC volume fraction from 6% to 10% led to a graded structure. Different properties of Al/SiC functionally graded composites yield 5.3 μm in grain size, HV 147 in microhardness and 0.2554 mm^3/m in wear rate based on these conditions.

(2) The homogeneity in recirculation of SiC particles is directly proportional to number of FSP passes. Through three FSP passes, a homogenous distribution of SiC particles in aluminum alloy matrix with strong interfacial bonding is obtained.

(3) In Al/SiC FG composite layer, the grain size is inversely proportional to the FSP pass number. The grain size is reduced from 10.1 (in the first pass) to 5.3 μm (in the third pass). It is considered that the vigorous stirring action of the tool by SiC particles prevents the grain growth of DRX grains of the matrix.

(4) The hardness of the Al/SiC functionally graded composite layer increases significantly with an increase in pass number. The maximum microhardness obtained for FG composites is HV 147 and that for as-received 6082-Al is HV 97. The increase in hardness of Al/SiC FG composite can also be attributed to grain size refinement. The dynamic recrystallization and Orowan strengthening effect are the factors that affect grain size refinement.

(5) The Al/SiC FG composites processed with three FSP passes show enhanced wear resistance compared to as-received 6082-Al, which is due to the addition of hard ceramic particles (SiC) and increased hardness. Wear mechanism on FG composite is a combination of abrasive and adhesive wear modes.

Acknowledgments

The authors thank Centre for Automation and Instrumentation (CAI), NIT Warangal for providing necessary computational facilities to carry out the work. The first author acknowledges research fellowship from NIT Warangal.

References

[1] KAWASAKI A, WATANABE R. Concept and P/M fabrication of functionally gradient materials [J]. Ceramics International, 1997, 23: 73−83.

[2] HUANG C Y, CHEN Y L. Design and impact resistant analysis of functionally graded Al_2O_3−ZrO_2 ceramic composite [J]. Materials and Design, 2016, 91: 294−305.

[3] NAEBE M, SHIRVANIMOGHADDAM K. Functionally graded materials: A review of fabrication and properties [J]. Applied Materials Today, 2016, 5: 223−245.

[4] MAHAMOOD R M, MEMBER E T A, SHUKLA M, PITYANA S. Functionally graded material : An overview [J]. Proceedings of the World Congress on Engineering, 2012, 3: 2−6.

[5] UDUPA G, RAO S S, GANGADHARAN K V. Functionally graded composite materials: An overview [J]. Procedia Materials Science, 2014, 5: 1291−1299.

[6] ERDEMIR F, CANAKCI A, VAROL T. Microstructural characterization and mechanical properties of functionally graded Al2024/SiC composites prepared by powder metallurgy techniques [J]. Transactions of Nonferrous Metals Society of China, 2015, 25: 3569−3577.

[7] WATANABE Y, YAMANAKA N, FUKUI Y. Control of composition gradient in a metal−ceramic functionally graded material manufactured by the centrifugal method [J]. Composites (Part A): Applied Science and Manufacturing, 1998, 29: 595−601.

[8] TILLMANN W, STANGIER D, LAEMMERHIRT I A, BIERMANN D, FREIBURG D. Investigation of the tribological properties of high-feed milled structures and Cr-based hard PVD-coatings [J]. Vacuum, 2016, 131: 5−13.

[9] LI L, SUN Q, BELLEHUMEUR C, GU P. Composite modeling and analysis for fabrication of FDM prototypes with locally controlled properties [J]. Journal of Manufacturing Processes, 2002, 4: 129−141.

[10] COSTANTINI M, JAROSZEWICZ J. 3D-printing of functionally graded porous materials using on-demand reconfigurable microfluidics [J]. Angewandte Chemie — International Edition, 2019, 58: 7620−7625.

[11] SAADATMAND M, MOHANDESI J A. Comparison between wear resistance of functionally graded and homogenous Al−SiC nanocomposite produced by friction stir processing (FSP) [J]. Journal of Materials Engineering and Performance, 2014, 23: 736−742.

[12] NEMAT-ALLA M M, ATA M H, BAYOUMI M R, KHAIR-ELDEEN W. Powder metallurgical fabrication and microstructural investigations of aluminum/steel functionally graded material [J]. Materials Sciences and Applications, 2011, 2: 1708−1718.

[13] GROVES J F, WADLEY H N G. Functionally graded materials synthesis via low vacuum directed vapor deposition [J]. Composites (Part B): Engineering, 1997, 28: 57−69.

[14] JAMALUDIN S N S, MUSTAPHA F, NURUZZAMAN D M, BASRI S N. A review on the fabrication techniques of functionally graded ceramic-metallic materials in advanced composites [J]. Scientific Research and Essays Review, 2013, 8: 828−840.

[15] ROSEN D, WEISS L. Layered manufacturing: Current status and future trends [J]. Journal of Computing and Information Science in Engineering, 2016, 1: 60−71.

[16] WĘGLOWSKI M S. Friction stir processing—State of the art [J]. Archives of Civil and Mechanical Engineering, 2018, 18: 114−129.

[17] ARURI D, ADEPU K, ADEPU K, BAZAVADA K. Wear and mechanical properties of 6061-T6 aluminum alloy surface hybrid composites ((SiC+Gr) and ($SiC+Al_2O_3$)) fabricated by friction stir processing [J]. Journal of Materials Research and Technology, 2013, 2: 362−369.

[18] MISHRA R S, MA Z. Friction stir welding and processing [J]. Materials Science and Engineering R, 2005, 50: 1−78.

[19] MA Z Y. Friction stir processing technology: A review [J]. Metallurgical and Materials Transactions A, 2008, 39: 642−658.

[20] HANGAI Y, OBA Y. Fabrication of A1050−A6061 functionally graded aluminum foam by friction stir processing route [J]. Metallurgical and Materials Transactions A, 2011, 42: 3585−3589.

[21] GANDRA J, MIRANDA R, VILAC P, VELHINHO A, TEIXEIRA J P. Functionally graded materials produced by friction stir processing [J]. Journal of Materials Processing Technology, 2011, 211: 1659−1668.

[22] MISHRA R S, MA Z Y, CHARIT I. Friction stir processing: A novel technique for fabrication of surface composite [J]. Materials Science and Engineering A, 2003, 341: 1−4.

[23] MIRANDA R M, SANTOS T G, GANDRA J, LOPES N, SILVA R J C. Reinforcement strategies for producing functionally graded materials by friction stir processing in aluminium alloys [J]. Journal of Materials Processing Technology, 2013, 213: 1609−1615.

[24] MORADI FARADONBEH A, SHAMANIAN M, EDRIS H, PAIDAR M, BOZKURT Y. Friction stir welding of Al−B_4C composite fabricated by accumulative roll bonding: Evaluation of microstructure and mechanical behavior [J]. Journal of Materials Engineering and Performance, 2018, 27: 835−846.

[25] PAIDAR M, ASGARI A, OJO O O, SABERI A. Mechanical properties and wear behavior of AA5182/WC nanocomposite fabricated by friction stir welding at different tool traverse speeds [J]. Journal of Materials Engineering and Performance, 2018, 27: 1714−1724.

[26] POL N, VERMA G, PANDEY R P, SHANMUGASUNDARAM T. Fabrication of AA7005/ TiB_2−B_4C surface composite by friction stir processing: Evaluation of ballistic behaviour [J]. Defence Technology, 2019, 15: 363−368.

[27] SHARMA D K, PATEL V, BADHEKA V, MEHTA K, UPADHYAY G. Fabrication of hybrid surface composites AA6061/(B_4C+MoS_2) via friction stir processing [J]. Journal of Tribology, 2019, 141: 1−10.

[28] PAIDAR M, OJO O O, EZATPOUR H R, HEIDARZADEH A. Influence of multi-pass FSP on the microstructure, mechanical properties and tribological characterization of Al/B_4C composite fabricated by accumulative roll bonding (ARB) [J]. Surface and Coatings Technology, 2019, 361: 159−169.

[29] GANGIL N, MAHESHWARI S, SIDDIQUEE A N, ABIDI M H, EL-MELIGY M A, MOHAMMED J A. Investigation on friction stir welding of hybrid composites fabricated on Al−Zn−Mg−Cu alloy through friction stir processing [J]. Journal of Materials Research and Technology, 2019, 8: 3733−3740.

[30] JAIN V K S, VARGHESE J, MUTHUKUMARAN S. Effect of first and second passes on microstructure and wear properties of titanium dioxide-reinforced aluminum surface composite via friction stir processing [J]. Arabian Journal for Science and Engineering, 2019, 44: 949−957.
[31] SINGH C V, PACHAURI P, DWIVEDI S P, SHARMA S, SINGARI R M. Formation of functionally graded hybrid composite materials with Al_2O_3 and RHA reinforcements using friction stir process [J]. Australian Journal of Mechanical Engineering, 2019, 17: 1−14.
[32] BARATI M, ABBASI M, ABEDINI M. The effects of friction stir processing and friction stir vibration processing on mechanical, wear and corrosion characteristics of Al6061SiO_2 surface composite [J]. Journal of Manufacturing Processes, 2019, 45: 491−497.
[33] CHARLES L. Leica microsystem [J]. Microscopy Today, 2015, 23: 7−17.
[34] PAIDAR M, SARAB M L. Friction stir spot welding of 2024-T3 aluminum alloy with SiC nanoparticles [J]. Journal of Mechanical Science and Technology, 2016, 30: 365−370.
[35] BARMOUZ M, BESHARATI M K, SEYFI J. On the role of processing parameters in producing Cu/SiC metal matrix composites via friction stir processing: Investigating microstructure, microhardness, wear and tensile behavior [J]. Materials Characterization, 2011, 62: 108−117.
[36] RATHEE S, MAHESHWARI S, SIDDIQUEE A N, SRIVASTAVA M. Investigating the effects of SiC particle sizes on microstructural and mechanical properties of AA5059/SiC surface composites during multi-pass FSP [J]. Silicon, 2019, 11: 797−805.
[37] ABDOLAHZADEH A, OMIDVAR H, SAFARKHANIAN M A, BAHRAMI M. Studying microstructure and mechanical properties of SiC-incorporated AZ31 joints fabricated through FSW: The effects of rotational and traveling speeds [J]. International Journal of Advanced Manufacturing Technology, 2014, 75: 1189−1196.
[38] ARAB S M, KARIMI S, JAHROMI S A J, JAVADPOUR S, ZEBARJAD S M. Fabrication of novel fiber reinforced aluminum composites by friction stir processing [J]. Materials Science and Engineering A, 2015, 632: 50−57.
[39] ELANGOVAN K, BALASUBRAMANIAN V, VALLIAPPAN M. Effect of tool pin profile and tool rotational speed on mechanical properties of friction stir welded AA6061 aluminium alloy [J]. Materials and Manufacturing Processes, 2008, 23: 251−260.
[40] EFTEKHARINIA H, AMADEH A A, KHODABANDEH A, PAIDAR M. Microstructure and wear behavior of AA6061/SiC surface composite fabricated via friction stir processing with different pins and passes [J]. Rare Metals, 2016, 39: 1−7.
[41] SATHISKUMAR R, MURUGAN N, DINAHARAN I, VIJAY S J. Role of friction stir processing parameters on microstructure and microhardness of boron carbide particulate reinforced copper surface composites [J]. Sadhana—Academy Proceedings in Engineering Sciences, 2013, 38: 1433−1450.
[42] SATO Y S, PARK S H C, KOKAWA H. Microstructural factors governing hardness in friction-stir welds of solid-solution-hardened Al alloys [J]. Metallurgical and Materials Transactions A: Physical Metallurgy and Materials Science, 2001, 32: 3033−3042.
[43] ARCHARD J F. Contact and rubbing of flat surfaces [J]. Journal of Applied Physics, 1953, 24: 981−988.

搅拌摩擦加工制备铝基梯度功能复合材料及表征

Venkatesh BIKKINA, Sadasiva Rao TALASILA, Kumar ADEPU

Department of Mechanical Engineering, National Institute of Technology, Warangal 506004, Telangana, India

摘　要：在 6082 铝板的凹槽中填充 SiC 颗粒(平均粒径为 27.5 μm)，用一种新型多步搅拌摩擦加工(FSP)法制备 Al/SiC 梯度功能复合材料(FGM)。为了得到预先设定的梯度结构，使用 3 种工具进行 FSP，每种工具的搅拌针长度不同，SiC 颗粒的体积分数也不同。FSP 在室温下进行，其工艺参数如下：1~3 道次、旋转速度为 900 r/min、前进速度为 20 mm/min。利用扫描电子显微镜(SEM)和三维光学显微镜对梯度功能样品的显微组织进行表征，且测试其耐磨性和显微硬度等力学性能。结果表明，随着 FSP 道次的增加，SiC 颗粒分散更加均匀，材料的显微硬度增加。与未加工的 6082 铝合金相比，经 3 道次加工后，其显微硬度提高 51.54%。添加 SiC 颗粒后，Al/SiC 梯度功能使复合材料的耐磨性提高。

关键词：梯度功能复合材料；搅拌摩擦加工；碳化硅；AA6082-T6；道次数

(Edited by Wei-ping CHEN)